Chaotic cascade model for turbulent velocity distributions

Christian Beck*
Institute for Physical Science and Technology and Laboratory for Plasma Research, University of Maryland, College Park, Maryland 20742

(Received 6 July 1993; revised manuscript received 22 November 1993)

A coupled map lattice is introduced that simulates the time evolution of velocity differences in fully developed turbulent flows. The model considered is an extension of the Langevin theory to chaotic driving forces acting on a self-similar cascade of spatial levels. Compared to full simulations of the Navier-Stokes equation, the amount of necessary computing time is negligible. Despite its simplicity, the model is in perfect agreement with experimentally observed results, provided the chaotic driving force is generated by the fully developed logistic map with parameter value $\mu=2$. The shape of the velocity distributions, the slight asymmetry, the stretched exponential tails, as well as the moment scaling exponents ζ_m, come out in precisely the same way as in experimental measurements of high Reynolds number flows.

PACS number(s): 05.45.+b, 47.27.Jv

I. INTRODUCTION

Understanding the spatiotemporal structure of turbulent fluid flows is a challenging problem of nonlinear science that still lacks a complete solution. A phenomenon of particular interest is the intermittent behavior of fully developed turbulent flows [1–27]. Let

$$u(r,t)=v_r(\mathbf{x}+\mathbf{r},t)-v_r(\mathbf{x},t) \tag{1}$$

denote the difference of the radial component of the velocity field at two points in the liquid that are separated by a distance r. It has been observed in several experiments that the probability distribution of u deviates from a Gaussian function [1–4]. In particular, for rather small r (in the dissipative range) the distribution possesses tails that are approximately (but not precisely) of exponential type. What is even more striking is the fact that in almost all experiments the probability distribution of u is observed to be slightly asymmetric, although the average of u is zero. This asymmetry results in the fact that all higher-order odd moments of u are negative [1,2]. A typical experimental result for r in the subinertial range is plotted in Fig. 1 (the experimental data are from [1]). The figure shows a probability density measured by Castaing, Gagne, and Hopfinger in a jet experiment at Reynolds number $\mathrm{Re}_\lambda=852$ for $r/\eta=167$, where η denotes the Kolmogorov length scale. The distribution is normalized and the horizontal axis is rescaled such that the variance satisfies $\langle u^2\rangle=1$. For comparison, the figure also shows a normalized Gaussian function with variance 1. One notices significant asymmetric deviations from the Gaussian function. There have been several theoretical attempts as well as a large number of numerical experiments to explain the shape of turbulent velocity distributions, but a truly satisfactory theory is still missing. Most previous models yield only qualitative agreement with experimental observations, whereas the quantitative agreement of, e.g., the asymmetry of the distributions is rather poor.

Direct simulations of the Navier-Stokes equation are certainly the most straightforward method to compare with the experiments, but presently only simulations up to Reynolds numbers $\mathrm{Re}_\lambda\approx 100$ are possible [5], whereas the experiments reach $\mathrm{Re}_\lambda\approx 3000$ [1]. Thus it is necessary to consider appropriate models that yield a better understanding of high Reynolds number flows. It should

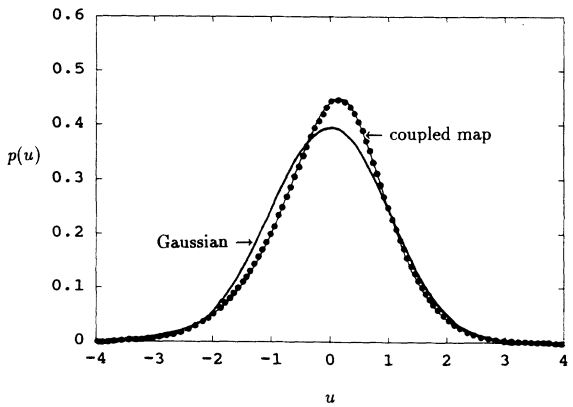

FIG. 1. Probability density of the velocity difference u as measured in a jet experiment at $\mathrm{Re}_\lambda=852$ for $r/\eta=167$ (dotted line). Also shown is a normalized Gaussian with standard deviation 1 (thick solid line). The thin solid line fitting the experimental data perfectly is a density obtained from the coupled map lattice introduced in Sec. II.

*Present address: Institute for Theoretical Physics, University of Aachen, RWTH, D-52056 Aachen, Germany.

be clear that full simulations of the Navier-Stokes equation can also be viewed as a type of experiment, representing—within the numerical accuracy—the true physics at low Reynolds numbers. The role of models (such as the one of this paper) is to provide a simplified setting in which some aspects of the turbulent dynamics can be better understood.

In this paper a very simple but physically well-motivated model for turbulent velocity differences at high Reynolds numbers will be introduced. The model is an extension of the Langevin theory to chaotic driving forces. These driving forces act on a self-similar cascade of spatial levels. The model is most conveniently formulated in terms of a coupled map lattice that also contains random ingredients, describing the fluctuations of the energy transfer from larger to smaller scales. The coupled map lattice is very easily implemented on a computer, and—compared to full simulations of the Navier-Stokes equation—the necessary amount of computing time is negligible. Despite this conceptual simplicity, the model yields probability distributions of turbulent velocity differences that are in perfect *quantitative* agreement with experimentally observed results, provided the driving force is generated by the fully developed logistic map (see, e.g., Fig. 1: the thin solid line, hardly visible behind the data points, is a density obtained from the coupled map lattice). This will be worked out for three different experiments at different Reynolds numbers and for various distances r. In particular, the asymmetry (skewness) of the distributions comes out in the correct way. The model also allows for some analytical treatment. For example, it can be shown that the average of u vanishes, whereas all higher odd moments of u are negative, in agreement with the experimental results. Finally, not only the probability distributions but also the scaling exponents ζ_m defined by the scaling relation

$$\langle u(r)^m \rangle \sim r^{\zeta_m} \tag{2}$$

come out correctly: They exhibit the well-known nonlinear dependence on m that has inspired the construction of many intermittency models [7–22]. Within the statistical error, the exponents obtained from the coupled map lattice coincide with the experimental results.

Although the approach described in this paper is new, the model still shares certain properties with previously introduced models, such as the random-β model of Benzi *et al.* [10,11], a Langevin model of Frisch and Morf [18], and the shell model studied by Jensen *et al.* [12–16]. A more detailed comparison with these and further models will be given in the conclusion.

This paper is organized as follows. In Sec. II the coupled map lattice will be introduced. In Sec. III the numerically obtained probability distributions are compared with the experimental data. Section IV deals with the extraction of the scaling exponents ζ_m. In Sec. V some analytical results are presented. Finally, the conclusion contains a brief comparison with previously developed models.

II. A COUPLED MAP LATTICE SIMULATING TURBULENT VELOCITY DIFFERENCES

The model that will be introduced in this section is based on a generalization of the Langevin theory to deterministic chaotic driving forces. For one-dimensional systems, this generalization has been described for the first time in [28] and has been further worked out in [29–33]. The relevant class of mappings are maps of Kaplan-Yorke type, first introduced in [34]. To simulate a turbulent flow, the approach of [28] has to be extended to infinite-dimensional (spatially extended) systems. Moreover, the self-similarity of the energy cascade as well as the random fluctuations of the energy transfer have to be taken into account. This will lead to the more advanced spatiotemporal model of the present paper. To make the paper self-consistent, some of the considerations of [28–30] will be rederived in the first part of this section.

Let us consider a fixed position $\mathbf{x}$ in the liquid and a fixed distance $\mathbf{r}$. We may then simply write $u(t)$ instead of $u(r,t)$. The dynamics of $u(t)$ is basically determined by two competing effects.

(i) In the absence of external or internal driving forces velocity differences tend to relax to the laminar state $u=0$. Thus we may write

$$\dot{u} = -\gamma u \ , \quad \gamma > 0 \ . \tag{3}$$

(ii) There are time-dependent chaotic forces in the turbulent liquid that drive the velocity differences and prevent the relaxation to the laminar state. Let us denote the resulting force (i.e., the difference of the forces at $\mathbf{x}+\mathbf{r}$ and $\mathbf{x}$) by $F(t)$. We obtain

$$\dot{u} = -\gamma u + F(t) \ . \tag{4}$$

Equation (4) looks similar to a Langevin equation modeling dynamical Brownian motion, but certainly there are major differences to this theory.

(i) The force $F(t)$ is not Gaussian white noise, but a chaotic force changing on a typical time scale τ.

(ii) The relaxation time scale γ^{-1} and the time scale τ of the force have comparable orders of magnitude.

(iii) In the Langevin theory u is the velocity. In our model u is the *velocity difference.*

From a numerical point of view, it is much easier to deal with chaotic mappings than with chaotic flows. For this reason, let us discretize the time and assume that the force $F(t)$ is a deterministic chaotic kick force given as follows:

$$F(t) = \sum_{n=1}^{\infty} \Phi(x_{n-1}) \delta(t - n\tau) \ , \tag{5}$$

$$x_{n+1} = T(x_n) \ . \tag{6}$$

Here T: $X \to X$ is a chaotic map on some phase space X and Φ is a function projecting from X onto the velocity space. The simplest choice one can think of is to take for T the logistic map $T(x)=1-\mu x^2$ on $X=[-1,1]$ and to choose $\Phi(x)=c(x-\langle x \rangle)$, where c is some coupling constant and $\langle x \rangle$ is the average of x_n. Once again let us remark that the analysis would apply in just the same way to any continuously varying chaotic flow $F(t)$, as generat-

ed, for example, by the Lorenz model or by the Navier-Stokes equation itself. The discrete model that is considered in Eq. (6) should be interpreted in the sense that we assume that smeared over a time scale τ, the integrated driving force varies chaotically in a similar way as the iterates of the logistic map or any other appropriate chaotic dynamics do. The discreteness just helps to make the theoretical and numerical analysis more convenient.

With the force (5), Eq. (4) can be integrated to give

$$x_{n+1}=T(x_n)\ , \tag{7}$$

$$u_{n+1}=\lambda u_n+\Phi(x_n)\ , \tag{8}$$

where $u_n:=u(n\tau+0^+)$ and $\lambda:=e^{-\gamma\tau}<1$. We obtain a map of Kaplan-Yorke type [34]. Much theoretical work has been done for maps of this type, dealing with various aspects of the system such as ergodic and mixing properties [30], the dimension of the attractor [29,33,34,35], higher-order correlation functions [32], and the Gaussian limit case obtained in a suitable scaling limit [28,29,31].

From now on we will use $\Phi(x)=x$ and assume that the average $\langle x\rangle$ vanishes, obtaining the simple form

$$\begin{aligned} x_{n+1}&=T(x_n)\ ,\\ u_{n+1}&=\lambda u_n+x_n \end{aligned} \tag{9}$$

of a dynamical system representing the deterministic analog of a linear Langevin dynamics. (Analogously, one can construct more general mappings corresponding to nonlinear Langevin equations; see [28,47].) Notice the fact that the force $F(t)$ is *not* Gaussian white noise but a complicated chaotic process. The kick strengths x_n evolve according to the mapping T in a deterministic way. As a standard example, we will typically choose for T the fully developed logistic map $T(x)=1-2x^2$.

Now let us extend the dynamical system (9) to incorporate spatiotemporal degrees of freedom. Quite similar to the β model introduced by Frisch, Sulem, and Nelkin [9] and further developed by Benzi, Paladin, Parisi, and Vulpiani [10], we assume that fully developed turbulence is characterized by the existence of a selfsimilar set of eddies on various scales. The various levels of this cascade are labeled by an index k. The larger k is, the smaller the size of the corresponding eddy. In the following we will often call an eddy at level k the "mother eddy" and the corresponding smaller eddies at level $k+1$ the "daughter eddies."

Let us denote by $u_n^{(k)}$ the velocity difference of two points in the liquid that are separated by a distance r_k, where r_k scales (in the inertial range) as

$$r_k=2^{-k}\ . \tag{10}$$

Moreover, let V_k denote the volume occupied by the active eddies at level k. On average, the active daughter eddies at level $k+1$ occupy only a certain fraction of the volume of the active mother eddies at level k:

$$V_{k+1}=\beta V_k\ ,\quad 0<\beta\le 1\ . \tag{11}$$

This is just the standard assumption of the β-model. For space-filling (Kolmogorov-like) eddies, $\beta=1$.

Our basic model assumption is that the momentum loss at level k serves as a chaotic driving force at level $k+1$. Moreover, a particular one of the daughter eddies at level $k+1$ gets only a random fraction $\xi_n^{(k)}$ of the momentum loss of the mother eddy at level k, the other part is transferred to other daughter eddies at level $k+1$. This can be expressed by the following coupled map lattice:

$$\begin{aligned} x_{n+1}&=T(x_n)\ ,\\ u_{n+1}^{(1)}&=\lambda_1 u_n^{(1)}+x_n\ ,\\ u_{n+1}^{(k)}&=\lambda_k u_n^{(k)}+c\xi_n^{(k-1)}(1-\lambda_{k-1})u_n^{(k-1)}\\ &\qquad (k=2,\ldots,K)\ . \end{aligned} \tag{12}$$

Here $\xi_n^{(k)}$ is a random variable on [0,1]. It is multiplied by a coupling constant c. Moreover, in order to be as general as possible, we allow the damping λ to depend on the scale, expressed by the index k. The simplest choice is to take for the $\xi_n^{(k)}$ uniformly distributed independent random variables, as generated by a pseudorandom number generator. But one may also generate them by the binary shift map or other strongly chaotic maps on the unit interval—the results presented in Sec. III do not depend on details of this choice.

The physical meaning of the coupled map lattice (12) is the following: During one time unit, the momentum loss of the mother eddy at level $k-1$ is $m_{k-1}(1-\lambda_{k-1})u_n^{(k-1)}$, where $m_{k-1}=\rho V_{k-1}$ is the mass associated with this eddy. A random fraction of this momentum (determined by the factor $\xi_n^{(k-1)}$) serves as a driving force for the daughter eddy at level k. The momentum balance for the daughter eddy is

$$m_k u_{n+1}^{(k)}=\lambda_k m_k u_n^{(k)}+\xi_n^{(k-1)}m_{k-1}(1-\lambda_{k-1})u_n^{(k-1)}\ . \tag{13}$$

Dividing by m_k we obtain

$$c=\frac{m_{k-1}}{m_k}=\frac{V_{k-1}}{V_k}=\beta^{-1}\ , \tag{14}$$

i.e., the coupling constant c is identified with the parameter β^{-1} of the β model.

The thin solid line in Fig. 1 shows a histogram of the variable $u_n^{(k)}$ at level $k=6$, obtained by iterating the coupled map lattice for $\lambda_k=\text{const}=0.85$ and $T(x)=1-2x^2$. The density is normalized and the horizontal axis is rescaled such that the variance satisfies $\langle u_n^{(k)2}\rangle=1$ (the dependence on the constant c is trivially absorbed by this rescaling). The curve is in perfect agreement with the experimentally measured velocity distribution (dotted line, the experimental data are from [1]). In particular, the asymmetric deviation from a normalized Gaussian function comes out in a quantitatively correct way. From this we conclude that the model system (12) is indeed a promising candidate to model velocity differences in fully developed turbulent flows. A systematic comparison with various experiments will be presented in the next section.

III. COMPARISON WITH EXPERIMENTS

To obtain a realistic model of a turbulent fluid flow valid for a large range of distances r, one has to specify how the parameters λ_k depend on the scale index k. The simplest choice, namely, constant λ_k, may be a reasonable approximation for the subinertial range, i.e., large distances r (see Fig. 1). However, it is well known that for smaller and smaller scales viscous effects become more and more dominant. Hence, for decreasing distances r, the damping γ is expected to increase, which means that $\lambda = e^{-\gamma(r)\tau}$ decreases. The easiest choice to model this increase of dissipation on smaller scales is to assume that γ changes linearly with the scale index k, or, in other words, that λ_k decreases exponentially:

$$\lambda_k = e^{-\gamma_0 \tau k} . \tag{15}$$

Since from Eq. (10) we have $k = -\ln r / \ln 2$, Eq. (15) is equivalent to a scaling law of the form

$$\lambda(r) = r^{\kappa} . \tag{16}$$

The exponent $\kappa = \gamma_0 \tau / \ln 2$ is expected to be nonuniversal, since it contains a typical time scale τ of the system. We estimate that κ is of the same order of magnitude as the inverse Reynolds number Re^{-1}, since

$$\gamma_0 \tau \sim \frac{\nu}{L^2} \tau \sim \frac{\nu}{vL} = \mathrm{Re}^{-1} . \tag{17}$$

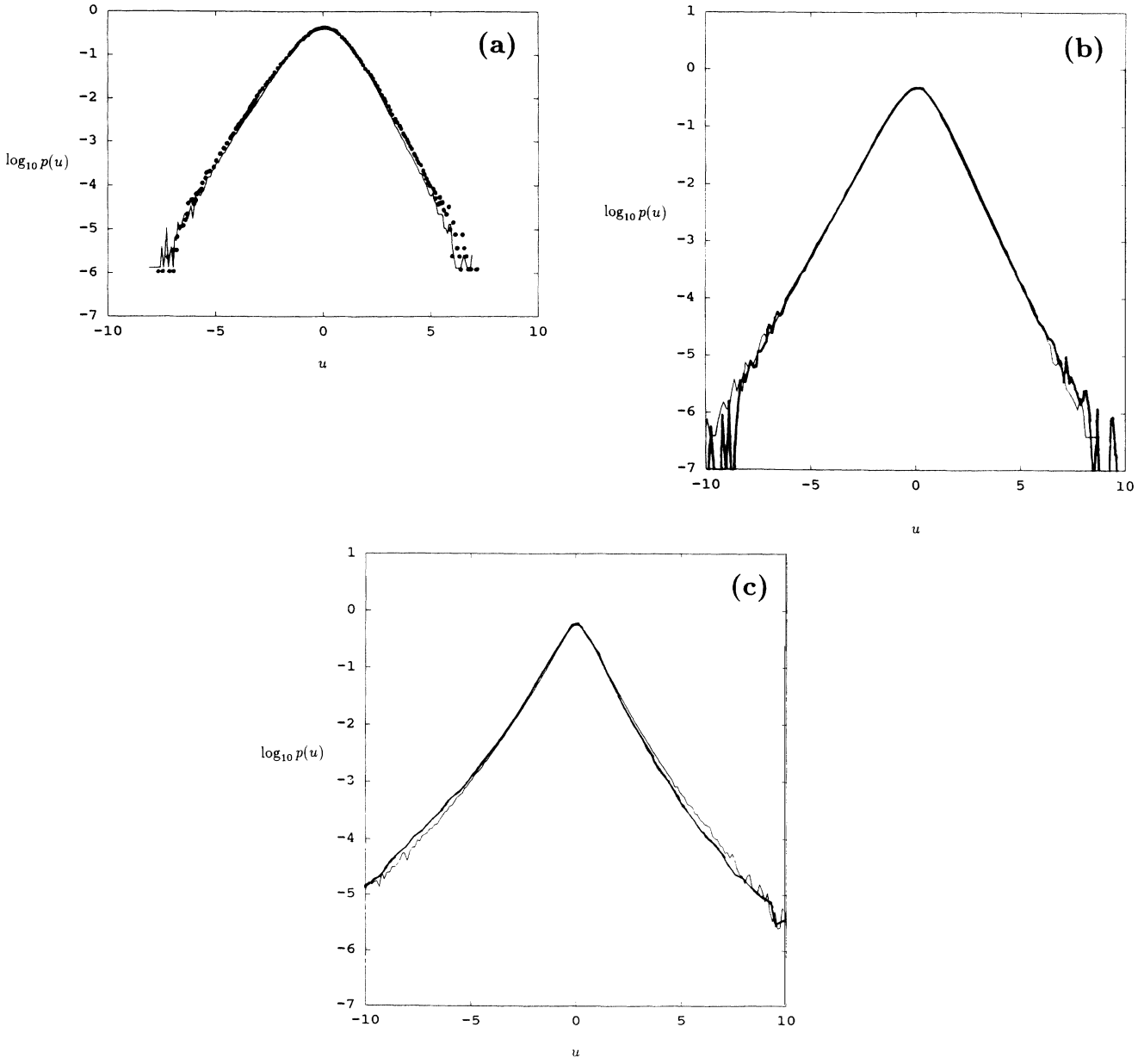

FIG. 2. Logarithm of the probability density of $u(r)$ measured for the jet experiment at (a) $r/\eta = 100$ (dotted line), (b) $r/\eta = 23.6$ (thick solid line), and (c) $r/\eta = 3.3$ (thick solid line). The figures also show probability densities obtained by iterating the coupled map lattice for $\gamma_0 \tau = 0.022$ and (a) $k = 7$, (b) $k = 10$, and (c) $k = 17$ (thin solid lines). Up to some stochastic fluctuations, the curves are almost identical.

Here ν denotes the kinematic viscosity, v is a typical velocity, and L is a typical length scale.

In the following we will use the coupled map lattice with parameters λ_k given by Eq. (15) to compare with experimentally observed velocity distributions. Nevertheless, other choices rather than the simple form (15) may also yield good results.

Figures 2(a)–2(c) show various probability distributions of velocity differences measured by Castaing, Gagne, and Hopfinger in the jet experiment at Reynolds number $\mathrm{Re}_\lambda = 852$ [1]. The distance r/η varies from $r/\eta = 100$ (a) to $r/\eta = 23.6$ (b) and $r/\eta = 3.3$ (c). On the other hand, the figures also show histograms obtained by iterating the coupled map lattice (12) for $\gamma_0 \tau = 0.022$,

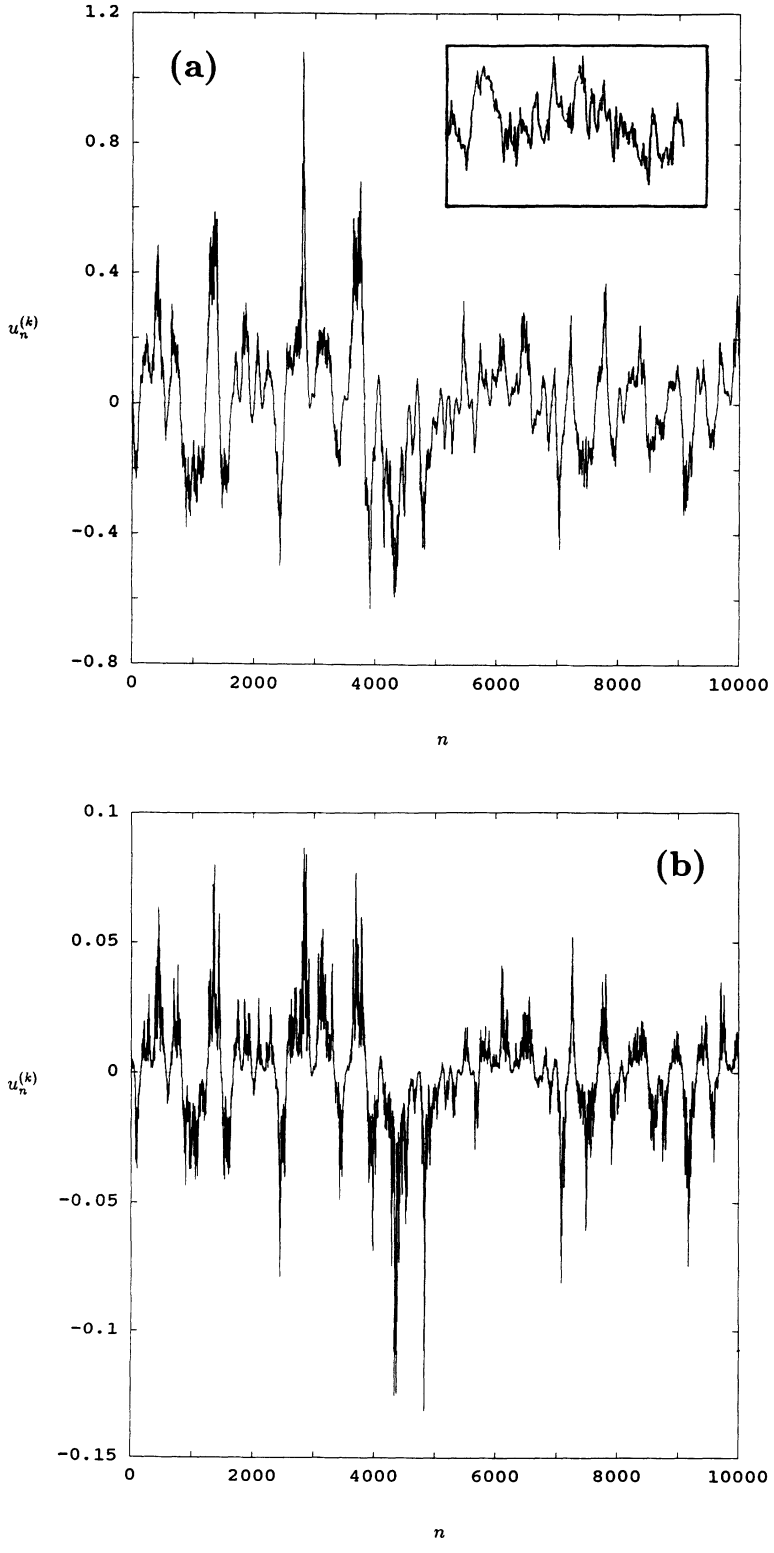

FIG. 3. Typical time evolution of the variable $u_n^{(k)}$ of the coupled map lattice for $\gamma_0 \tau = 0.022$ and (a) $k = 7$ and (b) $k = 17$. For comparison, the small window in (a) shows an experimentally measured velocity signal (from [4]).

$k=7$ (a), $k=10$ (b), and $k=17$ (c). As usual, we have chosen for the map T the fully developed logistic map. The quantitative agreement with the experimental data is remarkable; it is so good that the thin solid line corresponding to the coupled map lattice is often hardly visible [see, e.g., Fig. 2(b)]. One should also keep in mind that only two parameters are fitted: the parameter $\gamma_0\tau$ (roughly corresponding to Re^{-1}) and the index k of the lattice (determining the distance r). Just as in the experiment, where the Reynolds number is constant and the distance is varied, in our simulation we keep the parameter $\gamma_0\tau$ constant and vary the index k. Increasing k, we observe the typical transition scenario from distributions similar to a slightly asymmetric Gaussian function to distributions with stretched exponential tails. In contrast to many other intermittency models, the coupled map lattice yields the transition scenario in a *quantitatively* correct way, i.e., the simulated distributions coincide precisely with the experimentally measured distributions. Moreover, the amount of computing time necessary to generate the histograms with the coupled map lattice is much smaller than for other models.

In Fig. 3 a typical time evolution of the trajectory $u_n^{(k)}$ is plotted for $k=7$ (a) and $k=17$ (b). For small scales ($k=17$) we observe the typical intermittent outbursts that yield the stretched exponential tails of the distribution. For comparison, the small window in Fig. 3(a) shows an experimentally measured velocity signal in the wake of a circular cylinder [4]. The stochastic characteristics of the experimental signal looks very similar to that of the coupled map lattice.

Another experiment where probability distributions of velocity differences have been measured with high precision is a tunnel experiment at $\mathrm{Re}_\lambda=2720$ [1]. Figures 4(a)–4(c) show the distributions measured for $r/\eta=2971$ (a), $r/\eta=1307$ (b), and $r/\eta=11.6$ (c). Again it is possible to reproduce these distributions in a quantitatively correct way with the coupled map lattice, now with the parameter values $\gamma_0\tau=0.0069$ and $k=15$ (a), $k=16$ (b), and $k=31$ (c). As expected, the parameter $\gamma_0\tau$ has to be chosen smaller now. According to Eq. (17), it is proportional to Re^{-1}. Moreover, as expected for larger Reynolds numbers, we have to choose larger lattice sizes k to obtain quantitative agreement with the experiments, since the number of selfsimilar levels of the energy cascade is known to increase with increasing Reynolds number. Notice that relation (10) is well satisfied in the inertial range, whereas in the dissipative range the index k has to be increased slightly stronger in order to have optimum coincidence with the experiments, i.e., the cascade from mother to daughter eddies is run through more frequently in this range. Alternatively, we could replace Eq. (15) by a more complicated dependence, where the damping γ increases stronger in the dissipative range. In the noninertial range k is just regarded as a parameter that tells us how often the cascade from mother to daughter eddies is went through. In this range there is no simple scaling relation between r and k, and k has to be fitted to obtain optimum coincidence with the experiments.

Finally, as a third experiment we looked at a duct flow at $\mathrm{Re}_\lambda=515$ [2]. Again the experimentally observed

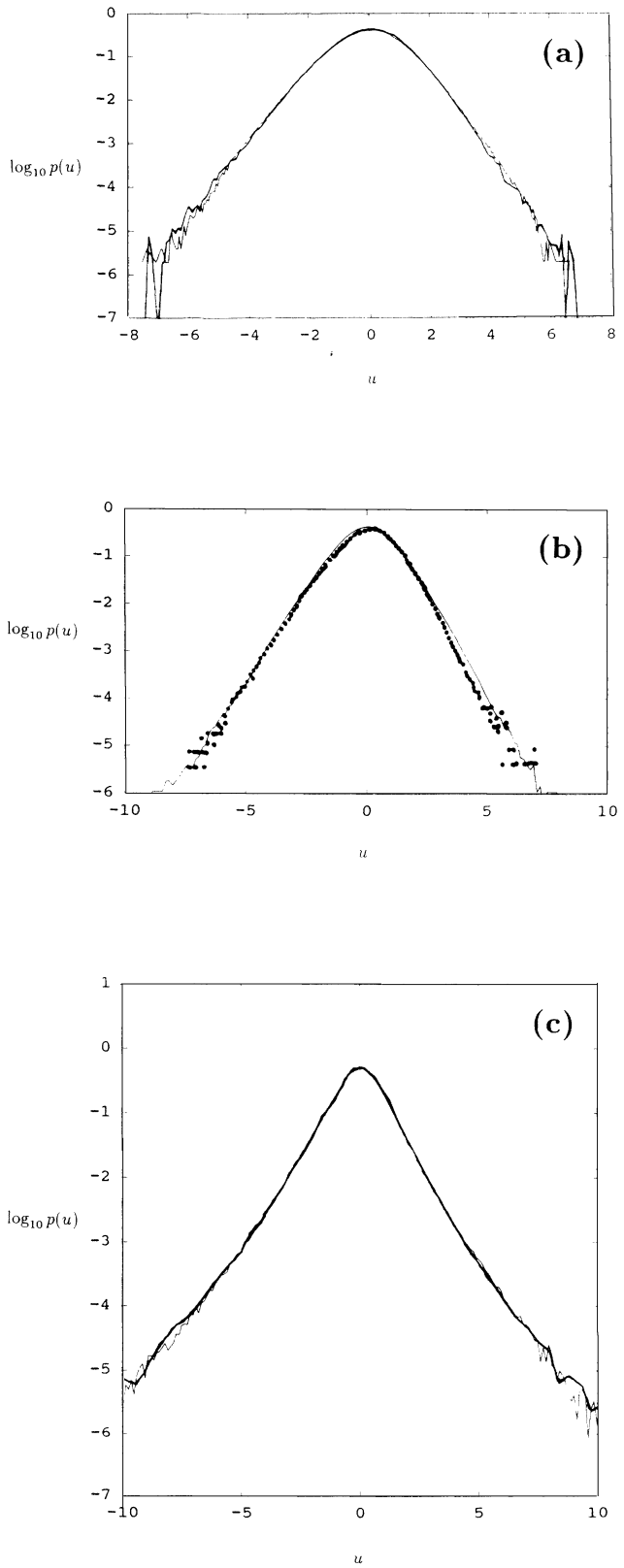

FIG. 4. Logarithm of the probability density of $u(r)$ measured for a tunnel experiment at $\mathrm{Re}_\lambda=2720$ and (a) $r/\eta=2971$ (thick solid line), (b) $r/\eta=1307$ (dotted line), and (c) $r/\eta=11.6$ (thick solid line). The experimental curves are very well reproduced by the coupled map lattice with $\gamma_0\tau=0.0069$ and (a) $k=15$, (b) $k=16$, and (c) $k=31$ (thin solid lines).

probability distributions can be exactly reproduced by the coupled map lattice (see Fig. 5), now with the parameters $\gamma_0\tau=0.025$, $k=6$ (a) and $k=8$ (b).

The three different experiments indeed confirm that the larger the Reynolds number, the smaller is the parameter $\gamma_0\tau$ and the larger is the necessary lattice size. But even for the largest experimentally accessible Reynolds numbers $\mathrm{Re}_\lambda \approx 3000$, the lattice size is still smaller than ~ 30. That means, finite-size effects of the lattice (i.e., of the energy cascade) still play an important role for experimentally accessible turbulent flows.

IV. THE MOMENT SCALING EXPONENTS ζ_m

In the absence of a theory for turbulent velocity distributions much of the theoretical and numerical work has been concentrating on the scaling behavior of the moments $\langle u(r)^m \rangle$ in the inertial range, where the various models [6–12] predict scaling behavior of the form

$$\langle u(r)^m \rangle \sim r^{\zeta_m} , \tag{18}$$

with different values for the exponents ζ_m. The ζ_m have been measured in several experiments [1–4], and in all these experiments a characteristic nonlinear dependence of ζ_m on m has been observed. The most popular explanation for this behavior is the multifractal approach of Benzi *et al.* [10], but also direct [5] and truncated [20] simulations of the Navier-Stokes equations as well as the shell model studied by Jensen *et al.* [12,15] confirm this specific nonlinear type of behavior.

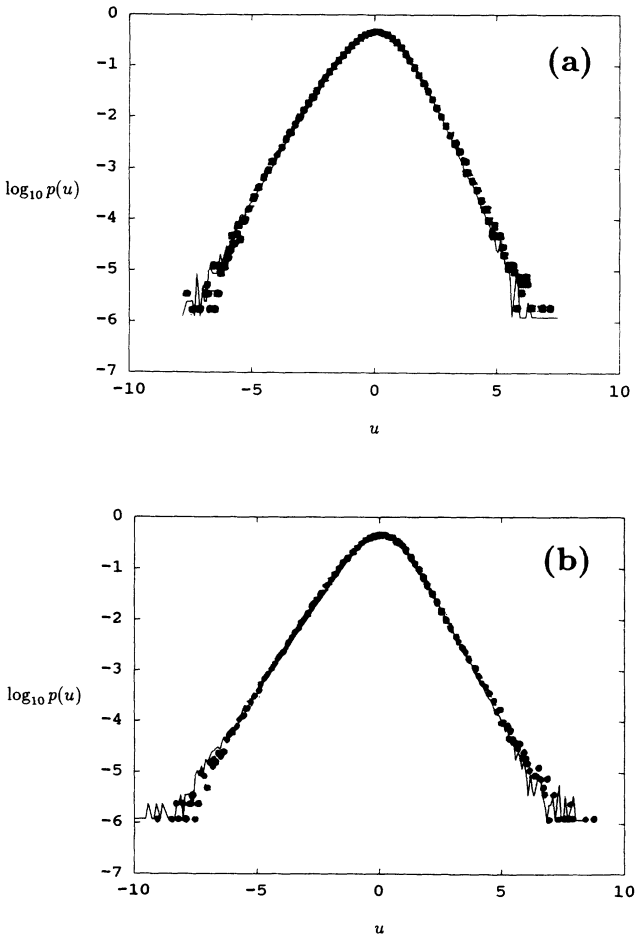

FIG. 5. Same as Figs. 2 and 4 for a duct flow at $\mathrm{Re}_\lambda=515$ and (a) $r/\eta=110$ and (b) $r/\eta=36.6$. The experimental measurements (dotted lines) coincide with probability densities obtained from the coupled map lattice for $\gamma_0\tau=0.025$, (a) $k=6$, and (b) $k=8$ (thin solid lines).

Our coupled map lattice does not only exactly reproduce the shape of the observed probability distributions, but also the scaling exponents ζ_m come out in a quantitatively correct way. It is remarkable that the model yields the correct exponents without fitting any parameters, except that we adjust the parameter β such that the generally accepted value $\zeta_3=1$ is reproduced.

The following numerical experiments was performed: The coupled map lattice (12) was iterated 5×10^6 times for $\gamma_0\tau=0.022$ (this parameter value corresponds to the jet experiment). The moments $\langle u^m \rangle$ were calculated as time averages (just as it is done in the experiments). We then plotted $\log_2|\langle u^m \rangle|$ versus $\log_2 r=-k$ and determined the slope in the inertial range $k\in[8,12]$ by linear regression. The constant $c=\beta^{-1}$ was adjusted in such a way that $\zeta_3=1$; then the other exponents ζ_m were determined with this value of the constant c. The experiment was repeated 5 times with different initial values and different random numbers to estimate the statistical error. The numerical results obtained by this method are listed in Table I and plotted in Fig. 6. The figure also shows the experimentally measured exponents by Anselmet *et al.* [2] and Meneveau and Sreenivasan [3], as well as the results obtained by Vincent and Meneguzzi [5] from a direct simulation of the Navier-Stokes equation. Within the statistical error, there is very good agreement between the coupled map lattice and the experiments and the direct simulation of the Navier-Stokes equation. For all experimental and numerical data plotted in the figure, the error is of the same order of magnitude as the vertical scattering of the symbols.

TABLE I. Scaling exponents ζ_m as obtained from the coupled map lattice.

m	ζ_m	Error
2	0.69	0.01
3	1	
4	1.28	0.02
5	1.54	0.02
6	1.79	0.03
7	1.97	0.06
8	2.18	0.07
9	2.28	0.14
10	2.46	0.19
11	2.54	0.24
12	2.72	0.22
13	2.80	0.34
14	2.97	0.31
15	3.06	0.43
16	3.23	0.39
17	3.34	0.52
18	3.51	0.48

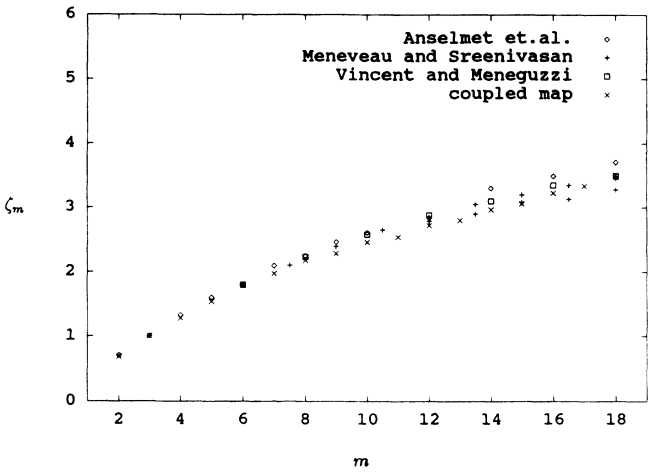

FIG. 6. Scaling exponents ζ_m versus m as obtained from the coupled map lattice. The figure also shows the experimentally measured exponents by Anselmet *et al.* [2] and Meneveau and Sreenivasan [3], as well as the numerical results obtained by Vincent and Meneguzzi [5].

Two remarks are in order.

(i) The constant $c=\beta^{-1}$ is nonuniversal. Choosing a different value $\gamma_0\tau$ (i.e., changing the experimental setup or the Reynolds number), one has to choose a slightly different c to adjust ζ_3 to the value 1. However, after this adjustment the scaling exponents ζ_m appear to be independent of $\gamma_0\tau$, at least within the statistical error. The variation of c with $\gamma_0\tau$ is actually rather small. For the jet experiment, $c^{-1}=\beta=0.582$, which is indeed close to the value $\beta=2^{-2/3}=0.630$ estimated by Benzi and Vulpiani [17].

(ii) The scaling behavior of the moments seems to be only approximate. For small m, a plot of $\log\langle u^m\rangle$ versus $\log r$ does not give a true straight line but a slightly curved line, for large m the fluctuations are huge. Both these phenomena are also observed for the experimental data [2]. One should therefore better call the exponents ζ_m "quasiexponents" since they describe an approximate scaling behavior for a lattice of finite size. Finite-size effects (finite Reynolds number effects) seem to be quite important to understand fully developed turbulent flows in a quantitatively correct way. The view that the scaling behavior of the moments is only approximate has also been emphasized in [1,36,37].

V. ANALYTICAL TREATMENT

The coupled map lattice introduced in Eq. (12) allows for some analytical treatment. This distinguishes it from other standard types of coupled map lattices studied in the literature, such as diffusively coupled logistic maps [38–42] or Henon maps [43]. For these types of examples the dynamics can typically be investigated by numerical means only, just in very rare cases it is also possible to obtain some analytical results [44–46]. For the system (12), on the other hand, several rigorous results can be proved. The reason is that the nonlinear chaotic behavior enters via the mapping T just at the top of the cascade ($k=1$). It is then propagated to smaller scales according to Eq. (12), which has a linear structure. Certainly it is also possible to add nonlinear terms to Eq. (12), i.e., to consider nonlinear generalizations of maps of Kaplan-Yorke type, where the term λu_n is replaced by a nonlinear function $g(u_n)$. For one-dimensional systems, this approach was introduced in [28] and further worked out (for special examples of g) in [47,48]. However, since already the simple linear form $g(u_n)=\lambda u_n$ yields a remarkably good agreement with the experiments, we will restrict the analysis of the present paper to the linear case $g(u_n)=\lambda u_n$.

To simplify the notation, let us define $c_k:=c(1-\lambda_k)$. The entire coupled map lattice can be written as

$$u_{n+1}^{(k)}=\lambda_k u_n^{(k)}+c_{k-1}\xi_n^{(k-1)}u_n^{(k-1)}\ ,\quad k=1,\ldots,K \tag{19}$$

if we agree upon denoting the iterates x_n of the map T as

$$x_n=:c_0\xi_n^{(0)}u_n^{(0)}\ . \tag{20}$$

For simplicity let us choose the initial values $u_0^{(k)}=0$, $k=1,\ldots,K$. Iterating the system (19), one notices that at each level k the variable $u_n^{(k)}$ can be written as a sum of iterates x_j multiplied by appropriate coefficients $a_j^{(k)}$:

$$u_n^{(k)}=\sum_{j=0}^{n-k}a_j^{(k)}x_j\ . \tag{21}$$

For example, at level $k=1$, one has

$$a_j^{(1)}=\lambda_1^{n-1-j} \tag{22}$$

(see also [30]). The question of interest is the following: Given the $a_j^{(k)}$, what are the $a_j^{(k+1)}$? Iterating Eq. (19), we get

$$u_n^{(k+1)}=c_k\sum_{j=1}^{n-1}\lambda_{k+1}^{n-1-j}\xi_j^{(k)}u_j^{(k)}\ . \tag{23}$$

Putting Eq. (21) into Eq. (23), we obtain after a short calculation

$$a_j^{(k+1)}=c_k a_j^{(k)}\sum_{i=k+j}^{n-1}\lambda_{k+1}^{n-1-i}\xi_i^{(k)}\ . \tag{24}$$

This yields

$$a_j^{(k)}=\lambda_1^{n-1-j}\prod_{s=1}^{k-1}\left[c_s\sum_{i_s=j+s}^{n-1}\lambda_{s+1}^{n-1-i_s}\xi_{i_s}^{(s)}\right]\ . \tag{25}$$

We recognize the following important result: Whatever the precise choice for the relaxation parameters λ_k and the random variables $\xi_n^{(k)}$, the velocity differences $u_n^{(k)}$ can be written in the form (21), where the $a_j^{(k)}$ are *positive* coefficients: $a_j^{(k)}>0$. The positivity follows from Eq. (25) and the fact that

$$\lambda_k=e^{-\gamma(k)\tau}>0\ , \tag{26}$$

$$\xi_n^{(k)}\in[0,1] \tag{27}$$

(we exclude the trivial case that all $\xi_n^{(k)}$ vanish). Moreover, since $\lambda_k<1$, the $a_j^{(k)}$ are bounded from above as well (for finite k).

For the fully developed logistic map, sums of the form (21) have been studied in detail in [32]. In particular, a graph theoretical method was introduced that yields a systematic procedure to calculate the moments and the invariant density of the $u_n^{(k)}$ in a perturbative way, provided the coefficients $a_j^{(k)}$ are given. In our case, the problem is slightly more advanced, since the $a_j^{(k)}$ are random variables rather than deterministic coefficients. There is a complicated interplay between expectations with respect to the invariant measure of T and expectations with respect to the random variables $a_j^{(k)}$. But, nevertheless, the techniques developed in [32] can still be used. In this paper, let us just apply one of the analytical results of [32], which is of particular physical interest. A more detailed mathematical analysis will be given elsewhere.

For a given realization of the random coefficients $a_j^{(k)}$, the moments of $u_n^{(k)}$ are given as

$$\langle u_n^{(k)m}\rangle=\sum_{j_1=0}^{n-k}\cdots\sum_{j_m=0}^{n-k}a_{j_1}^{(k)}\cdots a_{j_m}^{(k)}\langle x_{j_1}\cdots x_{j_m}\rangle \ . \tag{28}$$

Here $\langle\ \rangle$ denotes the expectation with respect to the natural invariant measure $d\nu$ of the dynamics T, which for $T(x)=1-2x^2$ reads

$$d\nu(x)=\frac{1}{\pi\sqrt{1-x^2}}dx \ . \tag{29}$$

The map T is conjugated to a Bernoulli shift [49]; the iterates can be written as

$$x_n=-\cos\pi 2^n u \ . \tag{30}$$

For the m-point function $\langle x_{j_1}\cdots x_{j_m}\rangle$ appearing in Eq. (28) one obtains

$$\begin{aligned}\langle x_{j_1}\cdots x_{j_m}\rangle&=\int_{-1}^{1}d\nu(x_0)x_{j_1}\cdots x_{j_m}\\&=(-1)^m\int_0^1 du\,\cos\pi 2^{j_1}u\cdots\cos\pi 2^{j_m}u \ .\end{aligned} \tag{31}$$

Writing $\cos\pi 2^{j_s}u=\frac{1}{2}(e^{+i\pi 2^{j_s}u}+e^{-i\pi 2^{j_s}u})$ and using the fact that for integers n

$$\int_0^1 du\,e^{2\pi i n u}=\begin{cases}1\ , & n=0\\ 0 & \text{otherwise}\ ,\end{cases} \tag{32}$$

one obtains [32]

$$\langle x_{j_1}\cdots x_{j_m}\rangle=(-1)^m 2^{-m}\sum_{\sigma}\delta(\sigma_1 2^{j_1}+\cdots+\sigma_m 2^{j_m},0) \ . \tag{33}$$

Here $\sum_\sigma$ means summation over all 2^m possible "spin" states $(\sigma_1,\ldots,\sigma_m)$ with $\sigma_i=\pm 1$, and the δ function denotes the Kronecker delta defined by

$$\delta(n,m)=\begin{cases}1\ , & n=m\\ 0 & \text{otherwise}\ .\end{cases} \tag{34}$$

Special well-known cases of Eq. (33) are $\langle x_j\rangle=0$ and $\langle x_{j_1}x_{j_2}\rangle=\frac{1}{2}\delta(j_1,j_2)$. Equation (33) implies the inequality

$$\langle x_{j_1}\cdots x_{j_m}\rangle\begin{cases}\geq 0\ , & m \text{ even}\\ \leq 0\ , & m \text{ odd}\ .\end{cases} \tag{35}$$

Notice that there are nontrivial higher-order correlations between the x_j. For example, from Eq. (33) we get

$$\langle x_j^2 x_{j+1}\rangle=-\tfrac{1}{4}\neq\langle x_j^2\rangle\langle x_{j+1}\rangle=0 \ . \tag{36}$$

In fact, for each $m\geq 2$ there is a certain set of tuples $(j_1,\ldots,j_m)$ (characterized by the graphs of [32]) where $\langle x_{j_1}\cdots x_{j_m}\rangle\neq 0$. For arbitrary realizations, the random coefficients $a_j^{(k)}$ appearing in Eq. (28) are positive. Thus Eq. (28) yields

$$\langle u_n^{(k)m}\rangle\begin{cases}=0 & m=1\\ >0 & m \text{ even}\\ <0 & m\geq 3 \text{ odd}\ .\end{cases} \tag{37}$$

This inequality remains valid if we finally perform the average over the random variables $\xi_n^{(k)}$ as well. Hence we have obtained a rigorous proof of the fact that all odd moments of u are negative, except the first moment (the average), which vanishes. Notice that this is just the characteristic feature of the moments measured in fully developed turbulent fluid flows: All higher odd moments are observed to be negative [2]. Notice also that if we had chosen for the x_n statistically independent random variables with average 0 rather than the iterates of the fully developed logistic map, all odd moments of u would vanish, and no asymmetry of the invariant density of u would arise at all. Thus the agreement with the experimental data would be much worse in this case. The asymmetry is due to the fact that there are complicated higher order correlations between the x_n, for example, those given by Eq. (36). In general, all these higher correlations are described by the graphs introduced in [32].

We may call this phenomenon a "dynamical symmetry breaking" effect: Although the map T as well as its invariant density is completely symmetric, the invariant density of u is not. Not only the existence of this asymmetry can be proved rigorously, but the numerical experiments of Sec. III also show that it comes out in a quantitatively correct way if one chooses for T the fully developed logistic map. From this one may conjecture that the dynamics $T(x)=1-2x^2$, conjugated to the Bernoulli shift in the sense of Eq. (30), plays a universal role for fully developed turbulent flows, in just a similar way as Feigenbaum's fixed point function [50] plays a universal role for the transition from ordered to chaotic states. Notice that all three different experiments can be fitted by the same mapping.

In [32] it was shown that among all smooth mappings conjugated to the $(\frac{1}{2},\frac{1}{2})$ Bernoulli shift the fully developed logistic map $T(x)=1-2x^2$ is distinguished: It possesses the largest possible number of tuples $(j_1,\ldots,j_m)$ for which the higher-order correlation functions $\langle x_{j_1}\cdots x_{j_m}\rangle$ vanish identically. For example, the binary

shift map $T(x)=2x \bmod 1$ with substracted mean has much more nonvanishing higher-order correlations: Here all even higher-order correlation functions are nonzero for arbitrary tuples $(j_1,\ldots,j_m)$, whereas for the fully developed logistic map most even higher-order correlation functions vanish identically (with the exception of those characterized by the graphs of [32]). In this sense the map $T(x)=1-2x^2$ can be regarded as a distinguished dynamical system that possesses the strongest random properties possible for a smooth deterministic system. This may serve as a hint why the coupled map lattice with this particular mapping yields such good agreement with the experiments: For a fully developed turbulent system we expect that the dynamics of the velocity field tends to a state where, although completely deterministic, it possesses the strongest possible random properties. For smaller Reynolds numbers, on the other hand, other mappings [such as the logistic map $T(x)=1-\mu x^2$ with $\mu<2$] may be more appropriate.

VI. CONCLUSION

In this paper a coupled map lattice has been introduced that simulates the time evolution of velocity differences u in fully developed turbulent flows. The model considered contains both chaotic and random ingredients. It yields probability distributions that deviate from a normalized Gaussian function in a way that is in perfect agreement with various turbulence experiments. In particular, the asymmetry of the distributions (the negativity of the odd moments) is reproduced correctly, and the stretched exponential tails characteristic for intermittent behavior are obtained in a quantitatively correct way. Moreover, the scaling exponents ζ_m characterizing the scaling behavior of the moments $\langle u(r)^m\rangle$ in the inertial range take on the same values as experimentally observed.

The model is based on an extension of the Langevin theory to deterministic chaotic driving forces, which act on a self-similar cascade of spatial levels. *A priori* the model can be studied for any type of chaotic driving dynamics, but we obtained by far the best agreement with the experimental measurements if the driving force is generated by a dynamical system conjugated to the Bernoulli shift, the fully developed logistic map $T(x)=1-2x^2$. In this case the negativity of the higher odd moments of u can be proved rigorously. The coupled map lattice is very easily implemented on a computer, and the necessary amount of computing time is several orders of magnitude smaller than for direct simulations of the Navier-Stokes equation.

Let us emphasize once more that, although the model could also be studied for independent random variables $T(x)=\pm 1$, such a simplified dynamics cannot account for the observed asymmetry of the probability distributions. Any symmetric stochastic process as a driving force yields just symmetric probability distributions. On the other hand, in Sec. III we showed that the map $T(x)=1-2x^2$ correctly reproduces the observed asymmetry for three different experiments, due to the dynamical symmetry breaking effect discussed in Sec. V. Although we cannot exclude the possibility that also other maps yield good results, the map $T(x)=1-2x^2$ seems to be ideally suited to model the stochastic properties of fully developed turbulent velocity signals in a quantitatively correct way. Of course, one could also replace the dynamics T by an asymmetric random process, such as, e.g., asymmetric dichotomous noise [51,52]. However, then the asymmetry is put in by hand, whereas in our model it arises quite naturally from the underlying chaotic dynamics.

Here we have just described the results obtained with a very simple coupling structure of the form given by Eq. (12). The model, however, can be easily extended to a more general setting. For example, one may wish to take into account a small backward scattering effect of the energy [53,54]. This can easily be achieved by adding to the right-hand side of Eq. (12) an additional term of the form $b\eta_n^{(k+1)}(1-\lambda_{k+1})u_n^{(k+1)}$, where the $\eta_n^{(k+1)}$ are further random variables, and $b \ll c$. This extended model then allows for some backward transmission of energy from smaller to larger scales. Spectral closure models also suggest that interactions of shells may go beyond those of nearest neighbors [55]. Such higher-order coupling terms could be easily introduced here as well. So far it is not clear whether direct simulations of the Navier-Stokes equation support long-range interactions in wave-number space [56–59]. Another possible generalization of the model is to let the parameters λ_k fluctuate in time or to generalize Eq. (3) to nonlinear evolution equations. On the other hand, we found it quite appealing that already the very simple form Eq. (12) yields such good coincidence with the experiments.

Let us compare the model with other previously introduced models. Frisch and Morf [18] consider a Langevin-like equation and point out that intermittency effects can be modeled by such a system if the driving force is a more complicated process than Gaussian white noise. This is also the basic idea of the present paper, just that the approach is extended to spatiotemporal systems and formulated in terms of a coupled map lattice, i.e., both space and time are discretized. The view that hydrodynamic behavior can be modelled by coupled map lattices has been emphasized by various authors; see, e.g., [38–42] and references therein. Even two-dimensional mappings often reveal typical intermittency features; see, e.g., [60,48].

The model introduced here shares certain properties with the β model of Frisch, Sulem, and Neikin [9] and the random β model of Benzi *et al.* [10], i.e., intermittency models based on multiplicative random processes [8]. In fact, the parameter β^{-1} is identified with the coupling constant c of the coupled map lattice [see Eq. (14)]. Very roughly, we may regard the model as a dynamical extension of the random β model, since now the velocity differences at level k obey a concrete evolution equation, which is not present in [10]. One may also introduce a more complicated (multifractal) probability distribution for the random variable $\xi_n^{(k)}$, as it is done in [10]. However, this is actually not necessary in our model, since even the simple choice of uniformly distributed $\xi_n^{(k)}$ yields perfect agreement with the experiments. In fact, the proba-

bility distributions plotted in Figs. 2, 4, and 5 appear to be quite independent of the distribution of the $\xi_n^{(k)}$; the most important property is just that the $\xi_n^{(k)}$ are positive and that they exist on a finite support. For example, we did not notice a significant difference if the uniform and independent $\xi_n^{(k)}$ are replaced by a chaotic dynamics $\xi_{n+1}^{(k)}=4\xi_n^{(k)}(1-\xi_n^{(k)})$, which generates a nonuniform density, and which possesses higher-order correlations. The distributions plotted in Figs. 2, 4, and 5 are also independent of the coupling c. This dependence is trivially absorbed by the condition that we look at distributions with standard deviation 1.

The approach of this paper also shares some of the ideas of Jensen, Paladin, and Vulpiani [12], namely, that fully developed turbulence can be modeled by a dynamical system of medium dimensionality d ($d\sim 20$–50) exhibiting chaotic behavior. Whereas Jensen, Paladin, and Vulpiani consider a continuous time dynamical system (previously introduced in [14,16]), the present approach is based on a discrete time dynamical system, which leads to a further simplification.

It is remarkable that the fully developed logistic map $T(x)=1-2x^2$ as a driving dynamics of the coupled map lattice yields such good results. As the iterates of T can be written as $x_n=-\cos\pi 2^n u$, i.e., as a cosine for which the frequency increases exponentially, we are somewhat reminded of the Fourier-Weierstrass ansatz chosen by Grossmann and Lohse [20], although this is just a formal analogy.

Finally, let us compare the model with the work of Castaing, Gagne, and Hopfinger [1], which inspired very much the development of the present paper. Castaing, Gagne, and Hopfinger consider an empirical model that fits the experimental data very well. However, the difficulty of their model is that it predicts a nonvanishing average of the velocity difference u, which has to be removed afterwards by an artificial shifting of the origin of the probability distribution. This difficulty does not arise for the coupled map lattice (12). Here the average $\langle u \rangle$ vanishes, and the asymmetry of the distribution (the negativity of the higher odd moments) arises naturally as an intrinsic property of the system.

ACKNOWLEDGMENTS

This work was started during the author's stay at the Niels Bohr Institute, Copenhagen. Most of the numerical work was done during a visit at the Institute for Theoretical Physics and the Institute for Solid State Physics, Eötvös University, Budapest. The final version was completed during the author's stay at the Institute for Physical Science and Technology and the Laboratory for Plasma Research at the University of Maryland, College Park. I would like to thank P. Cvitanović, T. Bohr, M. H. Jensen, P. Szépfalusy, T. Tél, J. A. Yorke, C. Grebogi, and E. Ott for the kind hospitality of their institutes and for several helpful remarks. Financial support by the Deutsche Forschungsgemeinschaft is gratefully acknowledged.

[1] B. Castaing, Y. Gagne, and E. J. Hopfinger, Physica D **46**, 177 (1990).
[2] F. Anselmet, Y. Gagne, E. J. Hopfinger, and R. A. Antonia, J. Fluid Mech. **140**, 63 (1984).
[3] Ch. Meneveau and K. R. Sreenivasan, J. Fluid Mech. **224**, 429 (1991).
[4] Ch. Meneveau, J. Fluid Mech. **232**, 469 (1991).
[5] A. Vincent and M. Meneguzzi, J. Fluid Mech. **225**, 1 (1991).
[6] A. N. Kolmogorov, C. R. Acad. Sci. USSR **30**, 301 (1941).
[7] A. N. Kolmogorov, J. Fluid Mech. **13**, 82 (1962).
[8] E. A. Novikov, Prikl. Mat. Mekh. **35**, 266 (1971) [Appl. Math. Mech. **35**, 231 (1971)].
[9] U. Frisch, P. L. Sulem, and M. Nelkin, J. Fluid Mech. **87**, 719 (1978).
[10] R. Benzi, G. Paladin, G. Parisi, and A. Vulpiani, J. Phys. A **17**, 3521 (1984).
[11] G. Parisi and U. Frisch, in *Turbulence and Predictability of Geophysical Flows and Climate Dynamics*, edited by M. Ghil *et al.* (North-Holland, New York, 1985).
[12] M. H. Jensen, G. Paladin, and A. Vulpiani, Phys. Rev. A **43**, 798 (1991); **45**, 7214 (1992).
[13] A. Crisanti, M. H. Jensen, G. Paladin, and A. Vulpiani, Phys. Rev. Lett. **70**, 166 (1993).
[14] R. Grappin, J. Leorat, and A. Pouquet, J. Phys. (Paris) **47**, 1127 (1986).
[15] R. Benzi, L. Biferale, and G. Parisi, Physica D **65**, 163 (1993).
[16] M. Yamada and K. Ohkitani, J. Phys. Soc. Jpn. **56**, 4210 (1987); Prog. Theor. Phys. **79**, 1265 (1988); Phys. Rev. Lett. **60**, 983 (1988).
[17] R. Benzi and A. Vulpiani, J. Phys. A **13**, 3319 (1980).
[18] U. Frisch and R. Morf. Phys. Rev. A **23**, 2673 (1981).
[19] B. B. Mandelbrot, J. Fluid Mech. **62**, 331 (1974).
[20] S. Grossmann and D. Lohse, Z. Phys. B **89**, 11 (1992); Physica A **194**, 519 (1993); Europhys. Lett. **21**, 201 (1993).
[21] I. Hosokawa and K. Yamamoto, Phys. Fluids A **2**, 889 (1990); **4**, 457 (1992).
[22] A. S. Monin and A. M. Yaglom, *Statistical Fluid Mechanics* (MIT Press, Cambridge, MA, 1975).
[23] G. K. Batchelor and A. A. Townsend, Proc. R. Soc. London Ser. A **199**, 238 (1949).
[24] R. M. Kerr, J. Fluid Mech. **153**, 31 (1985).
[25] R. H. Kraichnan, Phys. Rev. Lett. **65**, 575 (1990).
[26] A. B. Chhabra and K. R. Sreenivasan, Phys. Rev. Lett. **68**, 2762 (1992).
[27] E. D. Siggia, J. Fluid Mech. **107**, 375 (1981).
[28] C. Beck and G. Roepstorff, Physica A **145**, 1 (1987).
[29] C. Beck, Physica A **169**, 324 (1990).
[30] C. Beck, Commun. Math. Phys. **130**, 51 (1990).
[31] T. Shimizu, Physica A **164**, 123 (1990).
[32] C. Beck, Nonlinearity **4**, 1131 (1991).
[33] C. Beck and F. Schlögl, *Thermodynamics of Chaotic Systems* (Cambridge University Press, Cambridge, 1993).
[34] J. L. Kaplan and J. A. Yorke, in *Functional Differential Equations and the Approximation of Fixed Points*, edited

by H.-O. Peitgen and H.-O. Walther, Lecture Notes in Mathematics Vol. 730 (Springer-Verlag, Berlin, 1979), p. 228.
[35] R. Badii, G. Broggi, B. Derighetti, M. Ravani, S. Ciliberto, A. Politi, and M. A. Rubio, Phys. Rev. Lett. **60**, 979 (1988).
[36] L. C. Andrews, R. L. Philipps, B. K. Shivamoggi, J. K. Beck, and M. L. Joshi, Phys. Fluid A **1**, 999 (1989).
[37] I. Hosokawa, Phys. Fluids A **1**, 186 (1989).
[38] K. Kaneko, Prog. Theor. Phys. **72**, 480 (1984).
[39] R. Kapral, Phys. Rev. A **31**, 3868 (1985).
[40] J. P. Crutchfield and K. Kaneko, in *Directions in Chaos,* edited by B.-L. Hao (World Scientific, Singapore, 1987), Vol. 1, p. 272.
[41] T. Bohr and D. A. Rand, Physica D **52**, 532 (1991).
[42] T. Bohr, G. Grinstein, C. Jayaprakash, M. H. Jensen, J. Krug, and D. Mukamel, Physica D **59**, 177 (1992).
[43] A. Politi and A. Torcini, Phys. Rev. Lett. **69**, 3421 (1992).
[44] A. Bunimovich and Ya. G. Sinai, Nonlinearity **1**, 491 (1988).
[45] G. Keller, M. Künzle, and T. Nowicki, Physica D **59**, 39 (1992).
[46] V. M. Gundlach and D. A. Rand, Nonlinearity **6**, 165 (1993).
[47] C. Beck, G. Roepstorff, and C. Schroer, Physica D (to be published).
[48] J. Peinke, M. Klein, A. Kittel, A. Okninsky, J. Parisi, and O. E. Roessler, Phys. Scr. **T49**, 672 (1993).
[49] S. M. Ulam and J. von Neumann, Bull. Am. Math. Soc. **53**, 1120 (1947).
[50] M. J. Feigenbaum, J. Stat. Phys. **21**, 669 (1979).
[51] A. J. Irwin, S. J. Fraser, and R. Kapral, Phys. Rev. Lett. **64**, 2343 (1990).
[52] S. J. Fraser and R. Kapral, Phys. Rev. A **45**, 3412 (1992); J. Stat. Phys. **70**, 61 (1993).
[53] A. Brandenburg, Phys. Rev. Lett. **69**, 605 (1992).
[54] T. L. Bell and M. Nelkin, Phys. Fluids **20**, 345 (1977).
[55] R. H. Kraichnan, Phys. Fluids **30**, 1583 (1987).
[56] R. M. Kerr, J. Fluid Mech. **211**, 309 (1990).
[57] J. A. Domaradzki and R. S. Rogallo, Phys. Fluids A **2**, 413 (1990).
[58] J. A. Domaradzki, W. Liu, and M. E. Brachet, Phys. Fluids A **5**, 1747 (1993).
[59] F. Waleffe, Phys. Fluids A **5**, 677 (1993).
[60] L. Yu, E. Ott, and Q. Chen, Phys. Rev. Lett. **65**, 2935 (1990); Physica D **53**, 102 (1991).